Journal of the Iranian Chemical Society
https://doi.org/10.1007/s13738-018-1427-7

ORIGINAL PAPER

Synthesis and structural characterization for novel mixed-donor ligand palladium (II) based on graphene and oxime: its application as a highly stable and efficient recyclable catalyst

Samira Ashiri[1] · **Ebrahim Mehdipour**[1]

Received: 9 January 2018 / Accepted: 31 May 2018

Abstract

In this article, the palladium (II) mixed-ligand complex synthesized with reduced graphene oxides containing tetraethoxysilane and menthone oxime was used as an efficient solid catalyst for the Heck coupling reaction. To maintain stability and catalytic activity in the C–C bond reaction, graphene was considered due to the available surface as the solid support. Then, the structure of new heterogeneous catalyst was investigated by FT-IR, UV–Vis DRS, FE-SEM, EDX, AFM, XRD, ICP-OES, Raman, and TGA. The newly synthesized nanocatalyst have beneficial properties, including product's easy separation, the shorter time to react, purity products (yield 79–99%), and easier work-up procedure. Furthermore, the catalyst was reused six times without significant degradation in catalytic activity and performance.

Keywords Heterogeneous catalyst · Mixed-ligand palladium complex · Graphene oxides · Heck reaction · Solid support · Oxime

Introduction

Palladium (Pd) noble metal is a stable catalyst playing an indispensable role in organic synthesis due to its outstanding versatility and high activity. Palladium complexes have been considered as really useful and efficient choices for C–C coupling reactions. Pd-catalyzed coupling of aryl or vinyl halides and olefins, called as the Heck reaction, was one of the most effective ways to create a new C–C bond in various organic transformations [1–3]. The Heck coupling reaction provided a true path to assemble important vinylated olefins and arylated, and an extensive range of functional groups tolerance on both reactants allowed the appropriate usage in the final stage of total synthesis without protecting groups [4, 5]. In the past four decades, particular attention is paid to the use of palladium-catalyzed Heck cross-coupling reaction for organic and industrial synthesis such as natural products synthesis, active pharmaceutical intermediates, biologically active molecules, and modern chemical organic materials processes [6, 7]. Considering the importance of palladium complex, many homogeneous catalytic processes have significant disadvantages. These disadvantages include low catalyst stability [8–10], inability in catalyst recovery, and probabilistic toxicity due to remaining metal species [11], preventing their proper use in the reaction. On the other hand, homogeneous Pd catalysts lose their catalytic activity through accumulation and sedimentation, while with the emergence of heterogeneous catalysis, less product contamination and reusability of the precious catalysts can be achieved [12, 13].

Over the past decades, researchers have intensively studied the subject of dendritic catalysts proven on solid supports [14, 15]. In most cases, the dendritic catalyst has more positive effects than their non-dendritic analogs such as the improved catalytic activity of the heterogeneous dendritic catalysts. Several types of N-heterocyclic carbenes [16, 17] and nitrogen-based ligands [18] have been spread by proving them on solid supports. The most common solid support includes zeolite [19], metal oxides [20], silica starch [21], polymers [22], carbon nanotubes (CNTs) [23], clay [24], montmorillonite [25], and carbon derivatives [26], which are used to immobilize metal catalysts. Alternatively, these substrates are known to facilitate the catalyst recovery and recycling [27]. Functionalization of solid supports with showing chelating ligands appears to be a viable method

---

✉ Ebrahim Mehdipour
mehdipour.e@lu.ac.ir

[1] Department of Chemistry, Faculty of Science, Lorestan University, Khoramabad, Iran

to adjust their catalytic efficiencies and stabilize the metal complexes [28].

Lately, applications of graphene oxide (GO) and graphene (rGO) have been widely investigated by the development of metal-free carbon catalysts and the progress in graphene materials [29]. Graphene oxide nanosheet (GONS) is a flat monolayer two-dimensional sp^2-hybridized carbon material providing large surface area for interaction with other compounds [30]. It has attracted considerable attention during the past years due to their high thermal and mechanical stability as well as electrical conductivity and environmental friendliness. Functional groups on the GO sheets, according to availability, allow them to react to a wide range of compounds. This property of GO has highlighted it for potential applications in solid support catalysis [31]. These properties of GO led to its introduction as an efficient platform to load metals. These oxygen-containing groups on GO sheets had strong interactions with the organosilane to form functionalized GO. In this context, [3-(2 amino-ethylamino) propyl] triethoxysilanes (AATPES) were the most suitable molecules, which could behave as a linker in attaching $PdCl_2(oxime)_2$ complex to GO (Scheme 1).

Experimental

Materials and methods

All organic substrates and solvents purchased with purity 98% from Aldrich and Merck were used without further purification. The completion of reactions was monitored by the thin-layer chromatography (TLC) (hexane/EtOAc, 80:20). The FTIR spectrum of the products was recorded in a Bruker-Tensor320 spectrometer. In the range of 450–4000 cm^{-1}. The samples IR spectra were obtained using KBr tablet (weight ratio of 5/200 mg for samples: KBr). The catalysts structure were examined using patterns XRD. These patterns were recorded through a powder diffractometer, Holland Philips Xpert with Cu Kα radiation at a scanning op 2°/min from 10° to 90° (2θ). Surface structure and morphology of samples were studied using an LEO 440i scanning electron microscope at an operating voltage of 10 kV and under vacuum. Before measurements, the samples were coated by sputtering with a thin layer of gold. Absorption spectra UV–DRS of the sample were obtained using a Shimadzu UV–DRS 1650. TGA analyses were performed by a STA 409 apparatus (Linei) at a temperature from 0 to 800 °C with a 10 °C/min heating rate under nitrogen gas. The Pd content in the heterogeneous catalyst was determined using inductively coupled plasma optical emission spectroscopy (ICP-OES) conducted on a Perkin-Elmer 7300DV (Made in USA) model spectrometer. Elemental analysis was performed using an instrument model Flash EA 1112 Elemental Analyzer. Raman spectroscopy analyses were recorded on dispersive Raman Microscope with $\lambda_{exc} = 785$ nm and high spatial and spectral resolution at the position of the sample.

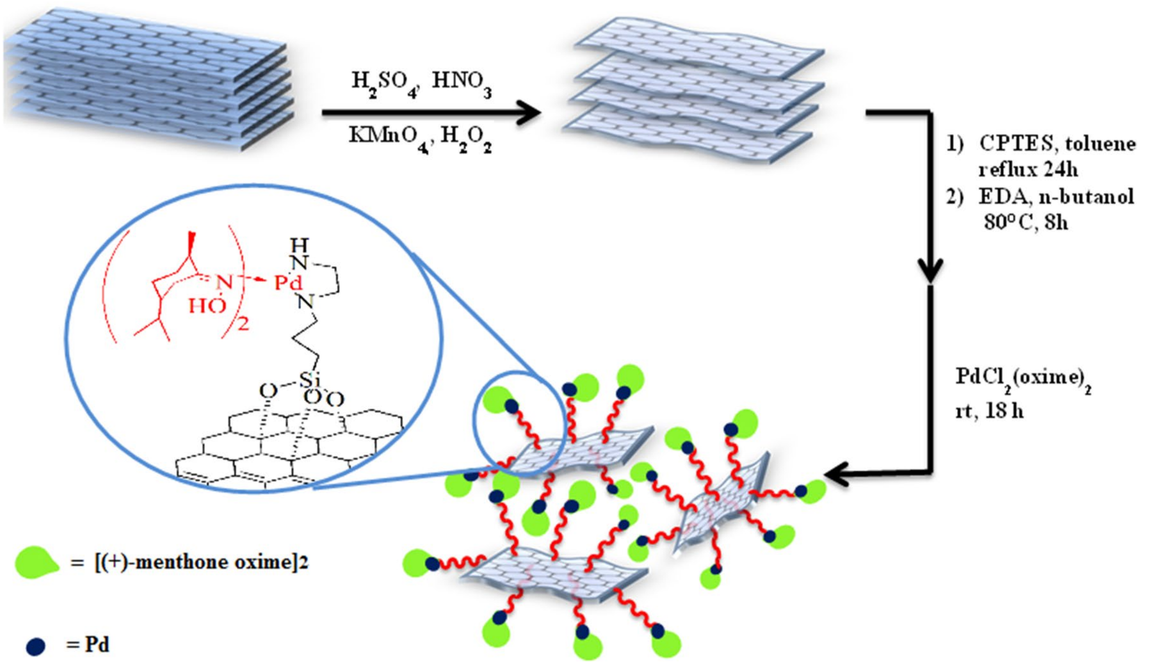

Scheme 1 Schematic illustration to prepare rGO-AATPES-$Pd(oxime)_2$ complex

Synthetic procedures

Synthesis of GO-AATPS

The GO was prepared from pure graphite using the Hummer's method. 2.0 g of GO powder was dispersed in 20 mL of toluene and sonicated for 10 min. The reaction was carried out with adding 3-chloropropyltriethoxysilane (CPETS: 4 mL) to suspension. The resulting mixture was stirred under reflux conditions for 24 h and then washed with toluene and ethanol (3×). The sample was dried at the temperature of 70 °C for 8 h. To prepare final GO-AATPES (AATPES: [amino-ethylamino]-propyltrimethoxysilane) on the surface of graphene oxide, 1.0 g of GO-CPTES was sonicated in 100 mL *n*-butanol and was added dropwise to 20 mL of ethylenediamine; the mixture of reaction was stirred at 85 °C for 10 h. After the performance of the reaction, the solid precipitate was washed several times with ethanol and then dried in a vacuum oven at 60 °C for a full day. CHNs: C%: 60.78, N%: 9.34, H%: 4.67.

Synthesis of menthone oxime

Menthone (2.15 mL, 1.314 mmol) was added to methanol (10 mL) containing sodium bicarbonate (1.5 g, 5.700 mmol) and hydroxylamine (1.12 g, 3.600 mmol). To the reaction mixture was added 1.25 mL water and refluxed for 3 h. Solution was diluted with water (12.5 mL) until all solids were dissolved. The organic layer was separated by adding hexane (25 mL) and this step was repeated three times, and the white crystals were formed after evaporation of the solvent. m.p: 55–56.5 °C, CHNs; C%: 71.37, N%: 8.61, H%: 11.23.

Synthesis of palladium complex with menthone oxime [$PdCl_2(oxime)_2$]

To prepare $PdCl_2$ (oxime)$_2$ complex, menthone oxime (0.156 g, 0.922 mmol) was added to methanol (7.3 mL). K_2PdCl_4 aqueous solution (50 mL) was then added dropwise and the suspension stirred whilst flask was covered with a lid. After, the mixture solvent was evaporated on rotavap for 18 h. The brown solid product was dissolved in acetone and dried in a vacuum. m.p: 59–60 °C, CHNs; C%: 46.32, N%: 5.36, H%: 7.216.

Synthesis of rGO-AATPES-Pd (oxime)$_2$ complex

In a two-neck flask, 0.5 g of GO-AATPES was dispersed in 20.5 mL of ethanol. Then 0.21 g of $PdCl_2$(oxime)$_2$ dissolved in 5 mL of methanol and gradually added to the mixture and stirred for 8 h under reflux conditions. The precipitate obtained was washed with water and ethanol. The solution was filtered and the precipitate was dried in a vacuum for 4 h at 40 °C (Scheme 1). The loading of palladium in the heterogeneous catalyst was determined using ICP-OES and EDX analyses. The concentration of palladium was 12.75 wt%, which was determined by ICP-OES. CHNs; C%: 56.67, N%: 7.38, H%: 6.85.

General procedure for Heck reactions

rGO-AATPES-Pd(oxime)$_2$ complex (0.15 mol%), aryl halide (1 mmol), olefin (2.2 mmol), and K_2CO_3 (1.5 mmol) in DMF (2 mL) were added to a flask armed with a magnetic stirring bar and the mixture stirred for the appropriate time until the reaction was complete. Progression of the reaction mixture was monitored by TLC (hexane/EtOAc, 80:20) at 110 °C. After completing the reaction, the catalyst was separated by filtration and then the solution diluted with EtOAc: water (15:15 mL). Then the organic layer was removed by a separatory funnel and dried in a rotavap (Scheme 2). Finally, the catalyst was reused for the same reaction. This process was repeated for six runs. The amount of catalyst leached was determined using inductively coupled plasma (ICP-OES).

Results and discussion

The catalytic activity rGO-AATPES-Pd(oxime)$_2$ was studied in the heck reaction on a laboratory scale. The catalyst preparation procedure is shown in Scheme 1. This process was characterized by UV–Vis, FT-IR, SEM, XRD, AFM, EDS, TGA, and Raman spectroscopy.

Structural characterization of the catalyst

All synthesized products were characterized by FT-IR analysis. Figure 1a shows the FT-IR spectrum of pure graphite. The graphene oxide FT-IR spectrum shows strong absorption bands at 3438, 2929, 1730, and 1642 cm^{-1}, which was related to –OH, C–H, C=O in –COOH group and non-oxidized carbon skeletal domains (C=C aromatic), respectively (Fig. 1b). In Fig. 1c, the bands at 722 and 556 cm^{-1} are relevant to the asymmetric and symmetric stretching vibrations of the C–Cl group. In addition, the stretching band at 2856 and 2927 cm^{-1} related to C–H *sp*^{2} and C–H *sp*^{3} groups the $(CH_2)_3$ propyl chains in the GO-CTPES. Also, the peaks at 1027 and 700 cm^{-1} correspond to O–Si stretching modes

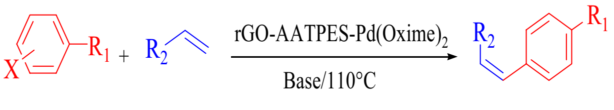

Scheme 2 Schematic illustration the heck reaction catalyzed by rGO-AATPES-Pd(oxime)$_2$ complex under mild conditions

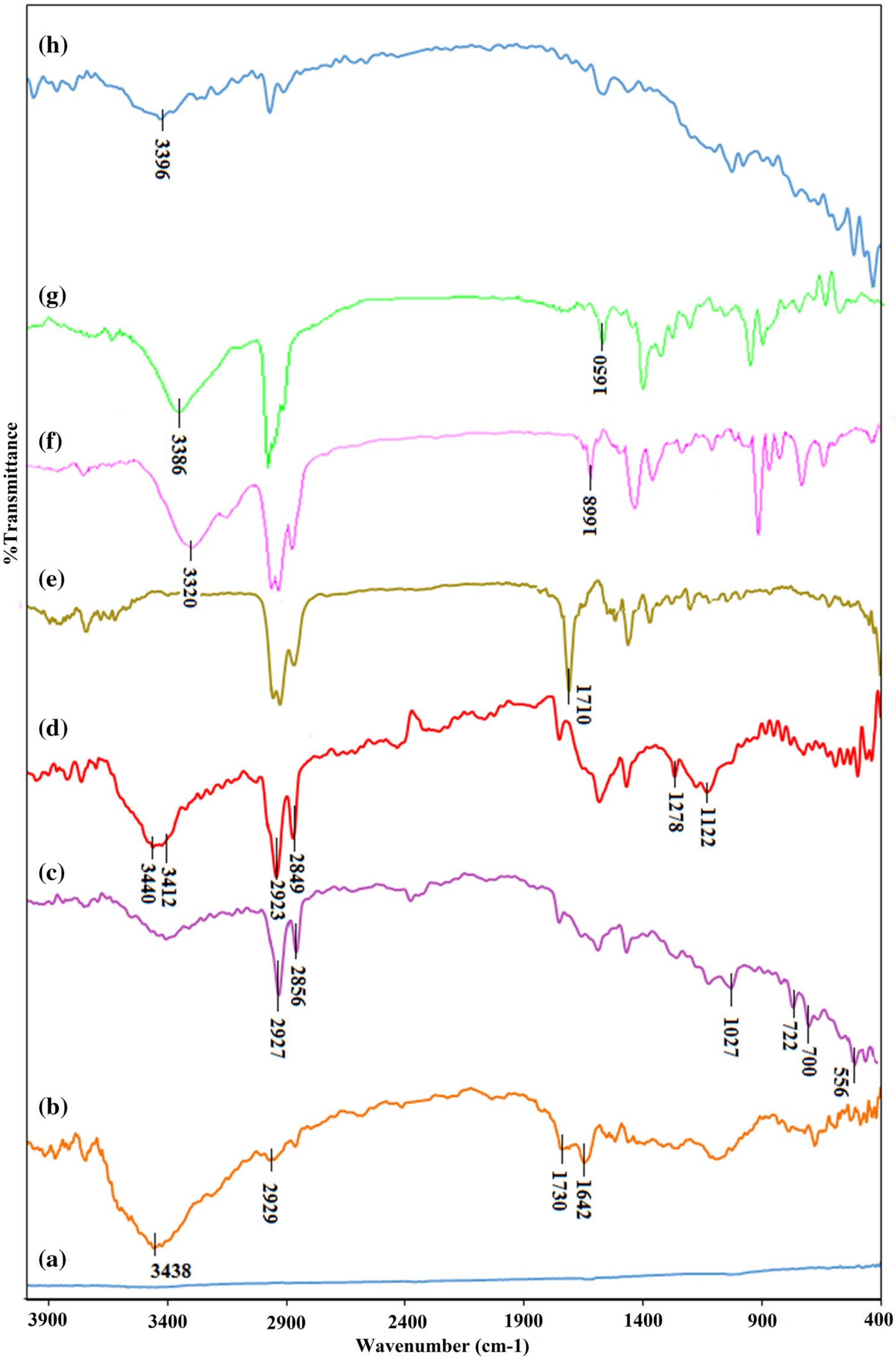

Fig. 1 FT-IR spectra for a graphite, b graphite oxide, c GO-CPTES, d GO-AATPES, e (s)-Menthone, f Menthone oxime, g $PdCl_2(oxime)_2$, and h rGO-AAPTES-$Pd(oxime)_2$

of GO-CTPES [32]. The characteristic peaks of the GO-AATPES in IR spectra are as followed: a sharp band at 3412–3440 cm^{-1} resulted from the stretching vibrations of NH_2 and N–H groups. These peaks at 2923–2849 and 1122–1278 cm^{-1} in Fig. 1d are relevant to the C–H and C–N stretching modes of GO-AATPES, respectively. Figure 1e, f shows the IR spectra of pure menthone and menthone oxime, respectively. The disappearance of the carbonyl group absorbance band at 1710 cm^{-1} and the appearance of oxime group absorbance band at 3320 cm^{-1} could be confirmed the synthesis of menthone oxime. Also, the peaks at 1668 cm^{-1} correspond to C=N stretching modes of menthone oxime. The $PdCl_2(oxime)_2$ FT-IR spectrum (Fig. 1g) shows that hydroxyl functional groups of menthone oxime were shifted

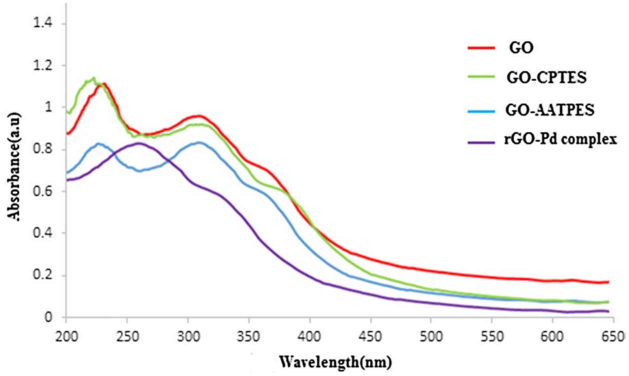

Fig. 2 UV–Vis DRS spectra of GO, GO-CPTES, GO-AATPES, and rGO-AATPES-Pd(oxime)$_2$

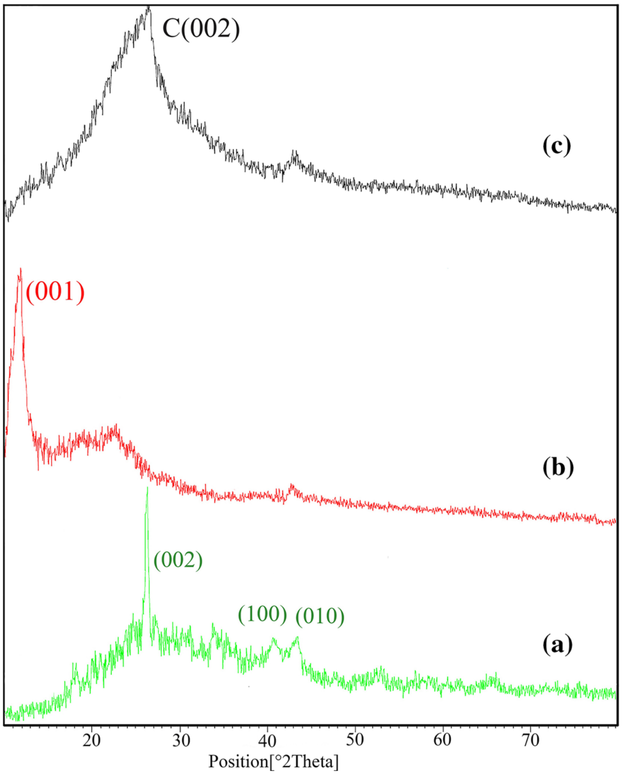

Fig. 3 XRD pattern of a graphite, b graphene oxide, and c rGO-AAPTES-Pd(oxime)$_2$ complex

to higher frequencies (3386 cm^{-1}) and peaks at 1650 cm^{-1} correspond to C=N [33]. Amin functional groups (–NH) of GO-AATPES were shifted to lower (3396 cm^{-1}). That, this transfer can be assigned to their more effective interactions with the palladium complex (Fig. 1h).

The formation of rGO-AATPS-Pd(oxime)$_2$ was investigated using UV–Vis diffuse reflectance spectroscopy (DRS) analysis. Figure 2 shows UV–Vis DRS of GO, GO-CPTES, GO-AATPES, and rGO-AATPS-Pd(oxime)$_2$. GO has shown a strong absorption peak with a shoulder at 240 and 329 nm (curve a), which corresponds to π–π* transition in the aromatic C=C bond and n–π* transition in the C=O groups [34]. However, the absorption peak at 240 nm redshifted to 261 nm which could be attributed to the reduced GO [35]. The first and second curves showed no change compared with the third curve during the reaction. Furthermore, the bands at around 240 and 329 nm in GO-AARPES spectra disappeared, which shows graphene oxide was indeed reduced by palladium complex [36].

The graphite XRD pattern shown in Fig. 3a diffraction peak at $2\theta = 43.11$ was corresponding to the (100) plane of the honeycomb structure of carbon and very strong diffraction peak at $2\theta = 26$ which is relevant to the (002) plane of graphite. Also as shown in Fig. 3b after oxidation, the diffraction peak has appeared at $2\theta = 11.71$ [with 0.8 nm interlayer spacing related to the (001) reflection], which indicates that GO has been fully oxidized. The XRD patterns of the rGO-AAPTES-Pd(oxime)$_2$ (Fig. 3c) showed peak corresponds to graphene. The diffraction peaks at $2\theta = 11.71°$ were disappeared and one new peak appeared at $2\theta = 26.8$ assigned to (002) reflections of rGO, indicating the reduction of GO in the presence of PdCl$_2$(oxime)$_2$ [36].

The morphology of GO and rGO-AAPTES-Pd(oxime)$_2$ complex was characterized by AFM, as shown in Fig. 4. AFM images revealed morphological variations between GO and rGO-AAPTES-Pd(oxime)$_2$ complex. Graphene oxide presented a nanosheet structure with several hundred nanometers large and 1.05 nm in thickness (Fig. 4a). While coated GO with complex (Fig. 4b) showed a thickness of 56.82 nm. The increased thickness of GO indicated the presence of a complex coating on GO surfaces.

One of the most useful tools for proving the structural characteristics and properties of graphene-based materials is Raman spectroscopy. Thus, it was used to study the changes that occurred in the crystal structure of the GO and rGO-AAPTES-Pd(oxime)$_2$ (Fig. 5). In Fig. 5a, Raman spectra of GO samples display two prominent peaks at 1343 and 1596 cm^{-1}, which is relevant to the D band and G band, respectively. The G band has corresponded to the first scattering of the E_{2g} phonon of sp^2-bonded carbon atoms in a 2D lattice. The D band suggests the presence of sp^3 defects (arising from a breathing mode of the aromatic rings). The spectral shifts which observed during reaction steps could be attributed to the derangement of the GO structure caused by the chemical interactions between functional groups of GO and other reactants. In Fig. 5b, G band of rGO-AAPTES-Pd(oxime)$_2$ complex (1587 cm^{-1}) shows redshifted compared with of GO (1596 cm^{-1}), which can be related to the interactions between GO and AATPES. To evaluate the quality of the graphite structure and to measure defects in the base graphene materials, the ID/IG (intensity ratio D band to G band) is used. The intensity ratio of the D and G

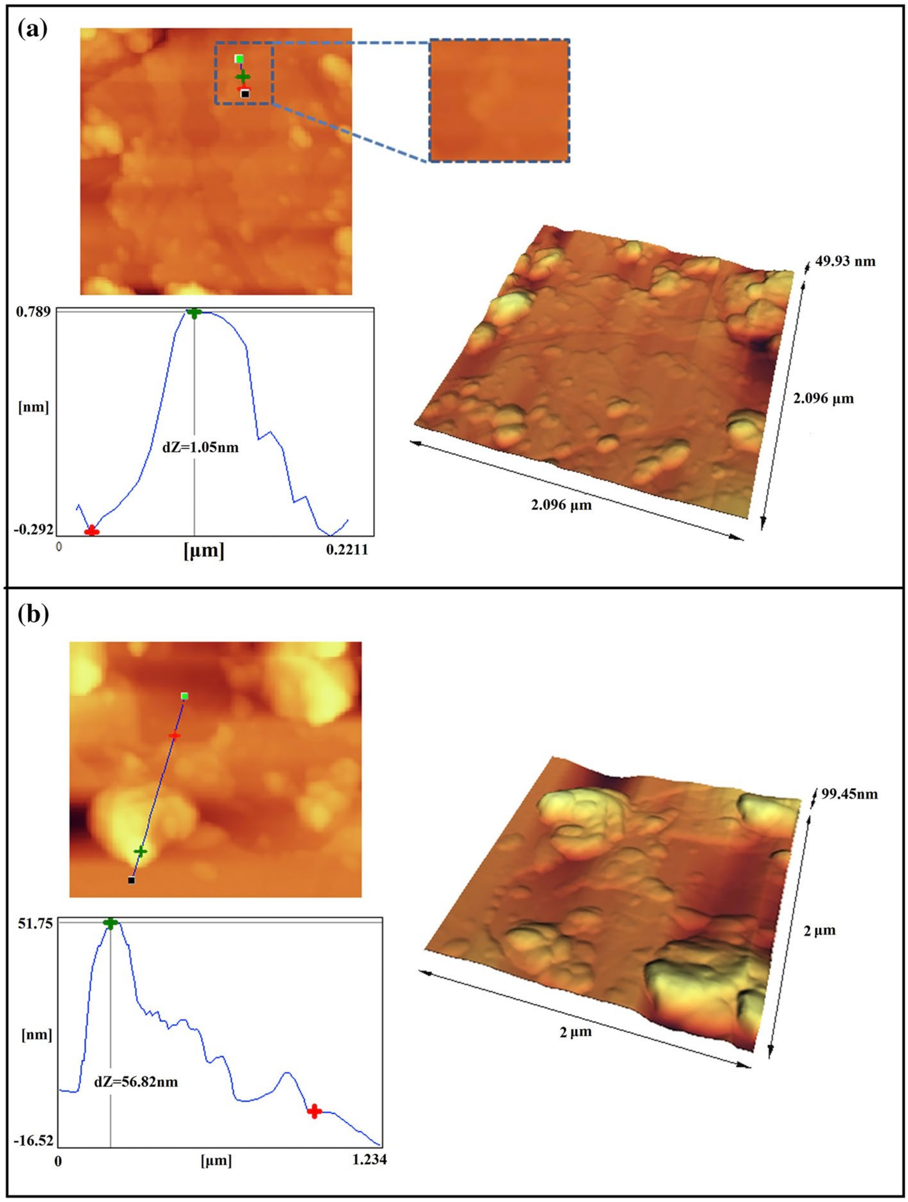

Fig. 4 The two- and three-dimensional AFM topography images, and corresponding height profiles of **a** GO and **b** rGO-AAPTES Pd(oxime)$_2$ complex

bands (ID/IG) improved from GO (0.957) to rGO-AAPTES-Pd(oxime)$_2$ (1.18). This increase is due to the decrease of the *sp*^{2} in-plane domain induced by the introduction of defects and disorder of the *sp*^{2} domain. Furthermore, the presence of Pd complex seems to cause structural defects and disorder of the GO sheets. These structural defects could play a significant effect in increasing the catalytic activity of the rGO-AAPTES-Pd(oxime)$_2$ catalyst [37, 38].

Scanning electron microscopy (SEM) was used for survey surface morphology and microstructures of modified graphene oxide. Figure 6a shows the uniform distribution of Pd(II) complex. SEM image in Fig. 6b showed the structure and morphology of natural graphite layers that were bonded by van der Waals forces. After oxidation, GO nanosheets were relatively exfoliated and wrinkled, that resulted in removing the interaction between sheets due to the presence of carboxylic, epoxy, and hydroxyl functional groups (Fig. 6c). Compared to the GO, GO-AAPTES showed more wrinkles and distance due to the presence of ethylenediamine (Fig. 6d). As observed from Fig. 6e, complex particles were attached to the edges and surface of graphene sheets.

Information about the chemical composition of the catalyst and the mass ratios of elements are measured by Energy Dispersive Spectroscopy (EDS). The EDX elemental analysis of the PdCl$_2$(oxime)$_2$ and rGO-AAPTES-Pd(oxime)$_2$ complex is shown in Fig. 7. The results further confirmed that PdCl$_2$(oxime)$_2$ was composed of carbon, nitrogen, oxygen, chlorine, and palladium (Fig. 7a) with mass ratios of 66.78, 9.84, 9.29, 8.98%, and 5.11 wt%, respectively. The ratio of chlorine, oxygen, and nitrogen is approximately

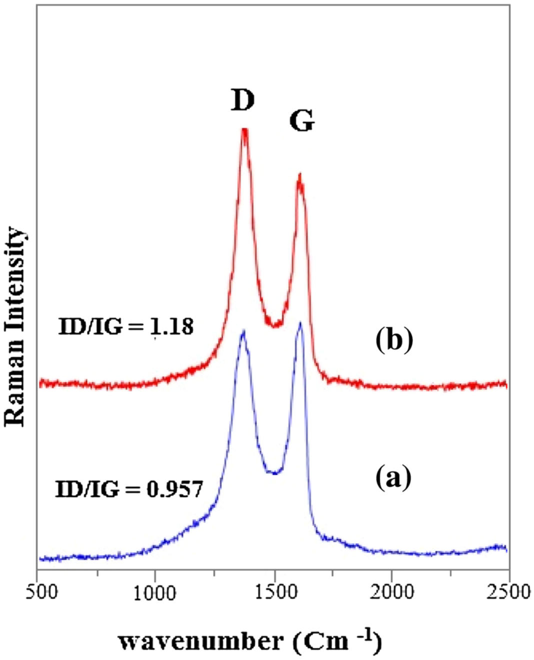

Fig. 5 Raman spectroscopy of a GO and b rGO-AATPES-Pd(oxime)$_2$

equal, but the proportion of palladium to each of the elements (O, N, Cl) is almost 1:2 ratio, that was confirmed to the synthesis of the compound PdCl$_2$(oxime)$_2$.

Also, the results further confirmed that the catalyst rGO-AAPTES-Pd(oxime)$_2$ was composed of carbon, nitrogen, oxygen, silicon, and palladium (Fig. 7c) with mass ratios of 48.24, 14.50, 17.80, 8.55%, and 10.91 wt%, respectively. The Si/Pd ratio (1:0.78) was higher than 1: 1 due to chemical reaction with edges and surface of graphene oxide during sample preparation. Furthermore, the element distribution maps (Fig. 7d) showed that the GO-AATPES sheets were densely functionalized with PdCl$_2$(oxime)$_2$ complex, reflecting the uniformity of the modification.

Both powdery samples GO and rGO-AAPTES-Pd(oxime)$_2$ are analyzed using TGA by heating the compounds from 0 to 800 °C at a heating rate of 10 °C min^{-1} under a nitrogen atmosphere (Fig. 8). As clearly seen from the graph in Fig. 8a, the GO at 100 °C exhibits about 12% weight loss and more than 42.3% loss between 110 and 210 resulting from the evaporation of water molecules that are trapped between the layers of GO and the decomposition of the labile oxygen-containing functional groups such as epoxy or hydroxyl groups, respectively. The third stage has shown 14.68% weight loss, which occurred at higher

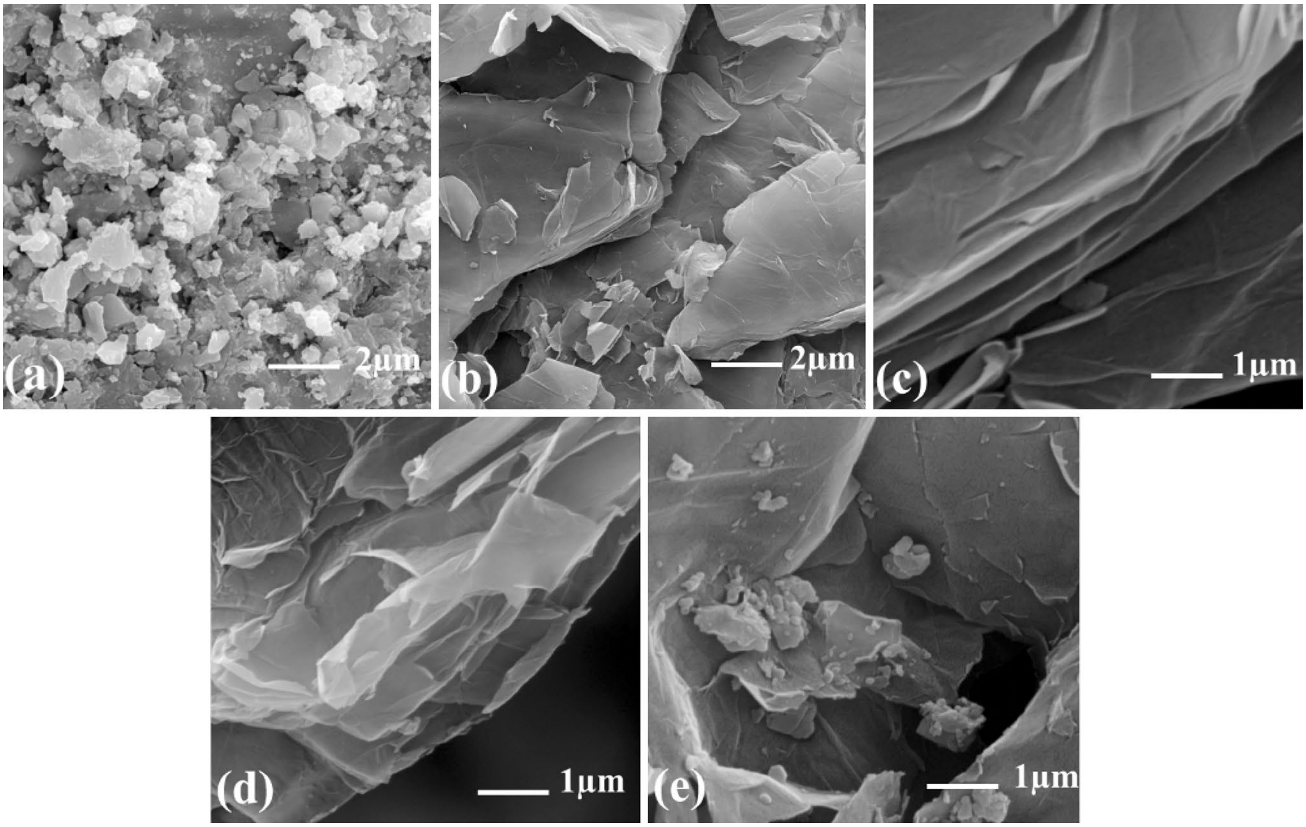

Fig. 6 FE-SEM images **a** PdCl$_2$(oxime)$_2$ complexes, **b** graphite, **c** graphene oxide (GO), **d** GO-AATPES, and **e** rG-AAPTES-Pd(oxime)$_2$ complex

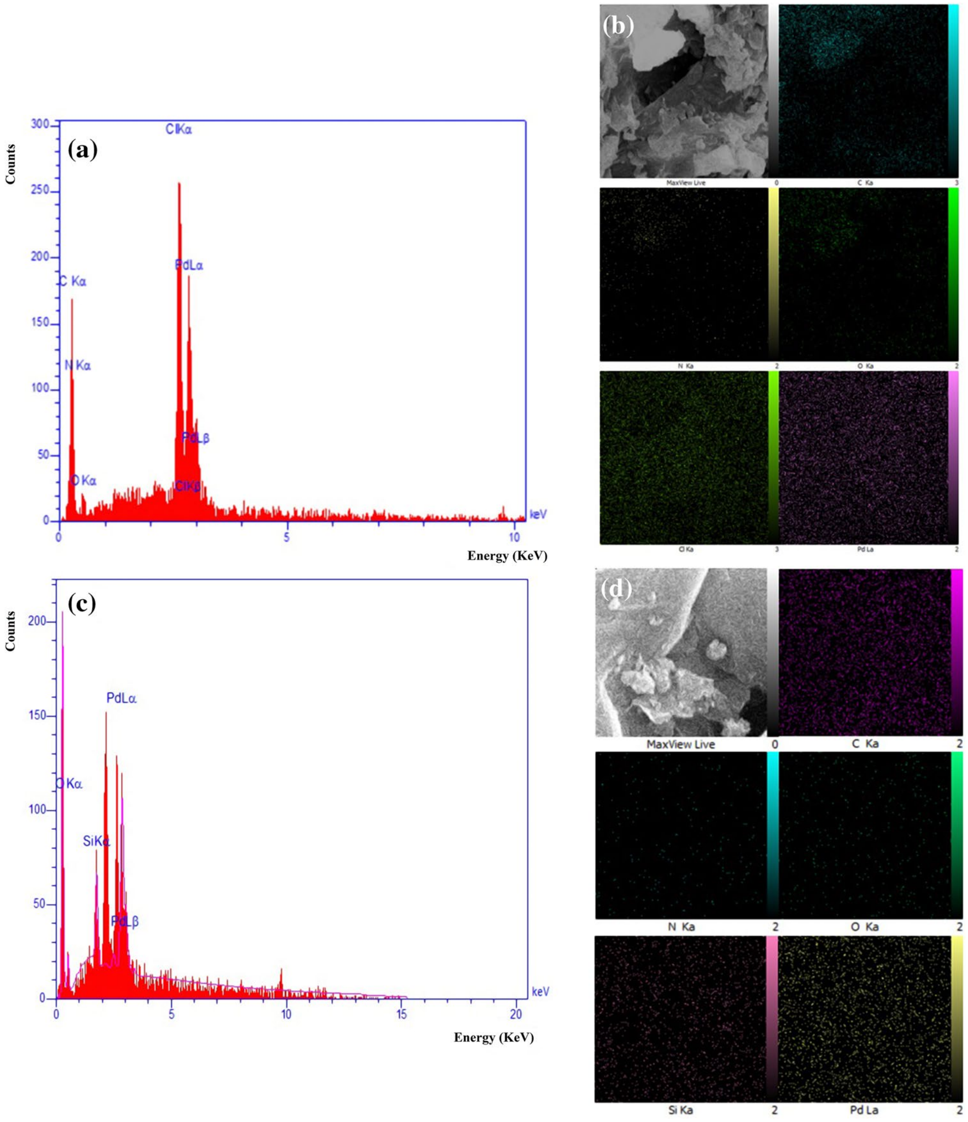

Fig. 7 The EDS spectrum of **a** $PdCl_2(oxime)_2$ and **c** rGO-AAPTES-$Pd(oxime)_2$ complex, elemental distribution maps in the **b** $PdCl_2(oxime)_2$ and **d** rGO-AAPTES-$Pd(oxime)_2$ complex region shown by EDX

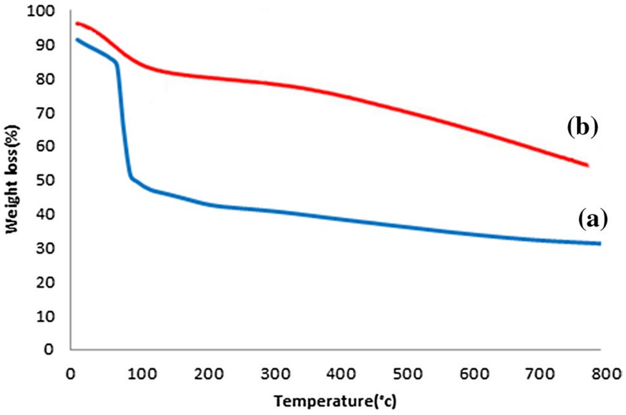

Fig. 8 TGA thermograms of **a** GO and **b** rGO-AATPES-$Pd(oxime)_2$

Table 1 Optimization of the reaction conditions for Heck reaction catalyzed by rGO-AAPTES-$Pd(oxime)_2$ complex

Entry	Solvent	Base	Cat. (mol%)	*T* (°C)	Yield (%)
1	MeCN	NEt_3	0.01	80	21
2	PhMe	NEt_3	0.02	90	34
3	THF	$NaHCO_3$	0.04	Reflux	40
4	THF	*t*-BuOK	0.06	Reflux	45
5	DMF	Na_2CO_3	0.08	100	85
6	DMF	K_2CO_3	0.1	120	75
7	DMF	K_2CO_3	0.12	120	90
9	DMF	K_2CO_3	0.15	110	**95**
11	DMF	K_2CO_3	0.18	110	91

Reaction conditions: rGO-AAPTES-$Pd(oxime)_2$ complex (0.15 mol %), aryl halide (1 mmol), olefin (2.2 mmol) ,and K_2CO_3 (1.5 mmol) in DMF (2 mL) at 110 °C temperature is due to the combustion of carbon skeleton in the GO [39]. In contrast, rGO-AAPTES-Pd(oxime)$_2$ has shown a higher thermal stability with a much lower mass loss up to 800 °C. The first mass loss in rGO-AAPTES-Pd(oxime)$_2$ (10%) which occurred at 100–110 °C and 15% at 220–300 °C was because of decomposition of the oxime and functional groups on graphene sheets and remains some oxygen functional groups on the surface rGO, respectively. The final mass loss which occurred at around 800 °C (35%) is due to the destruction of ring carbon. Also, it can be suggested that increasing the thermal stability of the catalyst is due to the presence of palladium on the rGO sheets.

Screening of reaction conditions

The efficiency of the Heck reaction depends on a variety of parameters, such as the solvent, temperature, base, structure of catalyst, and substrate nature. For optimizing the reaction conditions, different parameters were investigated on the synthesis of compound 3*d* that was selected as a model reaction. Initially, to evaluate the effect of the catalyst, different amounts of rGO-AAPTES-Pd(oxime)$_2$ complex were examined. As shown in Table 1, it was found that the highest yield was obtained using 0.15 g of the catalyst. There was no significant improvement in the yield by increasing the amount of catalyst (Table 1, entries 11).

Next, the effect of various solvents such as polar protic, aprotic solvents, and non-polar solvents such as MeCN, THF, DMF, and Toluene on the improvement of reaction was tested. The screening results presented in Table 1 showed that the polar aprotic solvent such as DMF obtained better results than other solvents. Hence, DMF solvent was preferred for further study. To investigate the effect of temperature on reaction, different temperatures were studied. The increase of reaction temperature in DMF solvent up to 110 °C led to high yield (Table 1, entry 5–11). Among all the investigated bases, the increase of the catalytic activity and high yields in the presence of K_2CO_3 were shown (Table 1, entry 11). After obtaining the optimum conditions for reaction, to investigate the scope and generality of this protocol, wide range aryl halides and olefins were used as substrates in the heck reaction. The results are shown in Table 2. In the Heck reaction, various substituents on olefins and aryl halides can influence on the rate of reaction. Electron-rich substituents (such as NH_2) on aryl halides cause to decrease the reaction rate, and conversely, electron-withdrawing substituents on aryl halides increase the reaction rate (Table 2, entries 3 and 9).

Also, the results from Table 2 show that aryl iodides produce the desired products in a shorter time than the aryl bromides and aryl chlorides. The reason is the difference in the carbon–halogen band that the increase in the length of the bond in the ariel iodide causes easier metal penetration and break the band. In the study of catalytic systems in coupling reactions, we find that aryl chloride is usually inactive in the reaction of the Heck with palladium, and only the iodine and brome react. Fortunately, the study of rGO-AATPES-Pd(oxime)$_2$ complex reveals appropriate results for aryl chlorides with proper yields.

Table 2 Heck cross-coupling reaction of aryl halides and olefins using catalyst rGO-AAPTES-Pd(oxime)$_2$

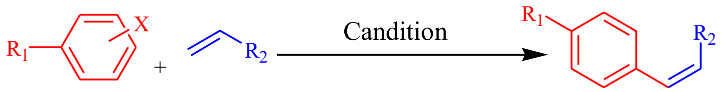

					Product	
Entry	Olefin	X	R_1	Time (min)	No.	Yield (%)
1	Styrene	I	H	30	3a	98
2	Methyl acrylate	I	H	35	3b	96
3	Methyl acrylate	I	NH_2	45	3c	92
4	Methyl methacrylate	I	H	40	3d	95
5	Acrylonitrile	I	H	30	3e	99
6	Methyl methacrylate	Br	H	65	3f	95
7	Styrene	Br	H	40	3g	97
8	Acrylonitrile	Br	H	35	3h	95
9	Acrylonitrile	Br	NH_2	35	3i	90
10	Methyl acrylate	Br	H	60	3j	93
11	Styrene	Cl	H	75	3k	85
12	Methyl methacrylate	Cl	H	80	3l	79

Reaction conditions: rGO-AATPES-Pd(oxime)$_2$ complex (0.15 mol%), aryl halide (1 mmol), olefin (2.2 mmol), and K_2CO_3 (1.5 mmol) in DMF (2 mL) at 110 °C

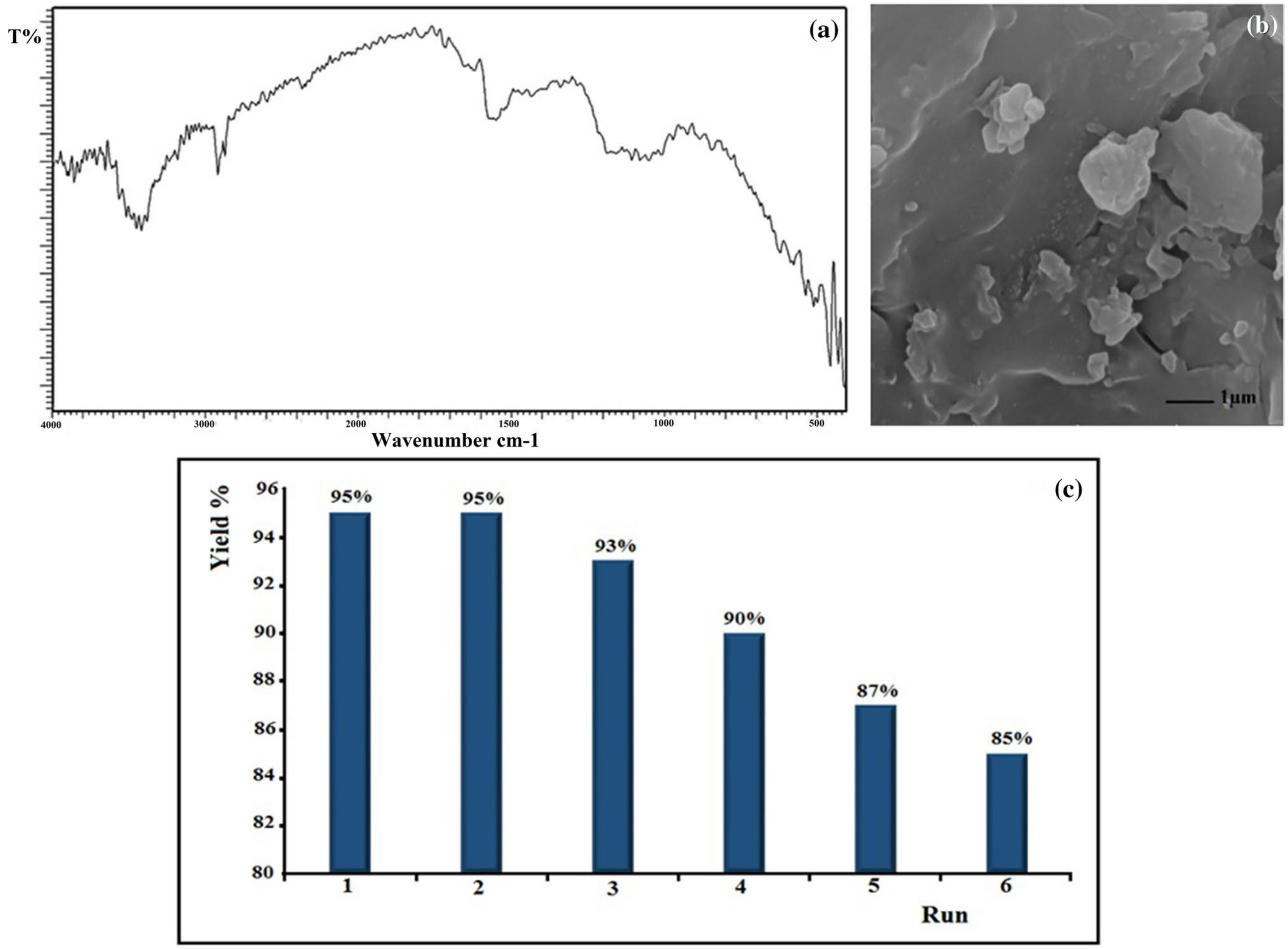

Fig. 9 **a** FT-IR. **b** FE-SEM. **c** Reusability of the catalyst for the synthesis of 3*d* (rGO-AATPES-Pd(oxime)$_2$ complex (0.01 mol%), aryl halide (1 mmol), olefin (2.2 mmol), and K_2CO_3 (1.5 mmol) in DMF (2 mL) at 110 °C

Table 3 Catalytic performance of different catalysts in the coupling reaction of iodobenzene, chlorobenzene, and bromobenzene with olefins

Entry	Catalyst	Conditions	X	Time (h)	Yield (%)	References
1	PdLn@β-CD	K_2CO_3, H_2O, reflux	Br, I	12, 4	90, 95	[41]
2	Pd/WO_3	Na_2CO_3, 120 °C	Br, I	5	85, 96	[42]
3	1-(9-Anthracenylmethyl)imidazole/$PdCl_2(MeCN)_2$	NMP, KOH, 160 °C	Cl, Br, I	5	79, 95, 99	[16]
4	Fe3O4@OA–Pd	n-Pr_3N, solvent free	Cl, Br	12, 7	81, 96	[43]
5	$Pd[(PhCH_2NH)(pC_6H_4OMe)PS_2]_2$	DMF, K_2CO_3, 100 °C	Br,I	8	86, 73	[7]
6	Pd/CoBDC	Et_3N, DMA, 90 °C	I	9	92	[44]
7	Co–NHC@MWCNTs	Li_2CO_3, PEG, 80 °C	Br, I	5	77, 85	[11]
8	rGO-AATPES-Pd(oxime)$_2$ complex	K_2CO_3, DMF, 110 °C	Cl, Br, I	1.25, 0.66, 0.5	85, 97, 98	This study

The aryl halides react with a variety of aliphatic and aromatic olefins with electron-withdrawing and donating group and giving the coupling products in good to excellent yields. It was observed that olefins with electron-withdrawing groups exhibit higher activity and reaction times of less relative to those bearing electron-donating groups on the olefin in the Heck reactions [40].

Reusability is one of the notable features environmentally and economically. Thereupon, reusability and recycling performance of the rGO-AATPS-Pd(oxime)$_2$ nanocatalyst were investigated under optimal conditions. The rGO-AATPS-Pd(oxime)$_2$ as a heterogeneous catalyst was recovered for six runs without significant loss of its activity. After the catalytic reaction, the catalyst was isolated by the filtration of the reaction mixture and washed with EtOH, and dried under vacuum at 80 °C for 2 h. The FT-IR and FE-SEM analyses of the catalyst after six periods indicated no detectable changes in the catalyst during the reaction of the recovery steps (Fig. 9). These results clearly indicate that the catalyst has high stability.

To get more information about the leaching of palladium in reaction, the reaction of iodobenzene with Methyl methacrylate as a model reaction was studied. After completion of the reaction and the workup for the first run, the amount of leaching was determined by ICP-OES analysis to be 12.75 wt%. The amount of Pd leaching after the six run was also determined by ICP-OES analysis to be only 9.85%, which indicates the stability of the catalyst during the reaction.

The comparison of the activity of the catalyst presented with various catalyst Pd in the Heck coupling reaction published in Table 3.

Conclusions

In summary, mixed-ligand rGO-AAPTES-Pd(oxime)$_2$ complex was successfully prepared and characterized through various analyses. The functionalized graphene complex was synthesized simply by reacting covalently to a reactive surfactant. Hence, this study highlighted that rGO had higher performance compared to other catalysts, since it is highly efficient and economical, and show increased activity at shorter reaction times and higher yields of products. The high stability and catalytic activity of this solid catalyst were related to Pd complexes. This method was efficient and simple, and is expected to be a useful synthetic protocol for synthesis of a wide range of novel chemical organic materials.

Acknowledgements The authors thank the Lorestan University Research Council for the support of this work.

References

1. M.R. dos Santos, R. Coriolano, M.N. Godoi, A.L. Monteiro, H.C. de Oliveira, M.N. Eberlin, B.A. Neto, New J. Chem. **38**, 2958 (2014)
2. Y. Zhu, J. Bai, J. Wang, C. Li, RSC Adv. **6**, 29437 (2016)
3. K.R. Balinge, P.R. Bhagat, Comptes Rendus Chimie **20**, 773 (2017)
4. R.P. Jumde, M. Marelli, N. Scotti, A. Mandoli, R. Psaro, C. Evangelisti, J. Mol. Catal. A Chem. **414**, 55 (2016)
5. E. Mohammadi, B. Movassagh, J. Mol. Catal. A Chem. **418**, 158 (2016)
6. H.-P. Gong, Z.-J. Quan, X.-C. Wang, Tetrahedron **72**, 2018 (2016)
7. K. Gholivand, R. Salami, K. Farshadfar, R.J. Butcher, Polyhedron **119**, 267 (2016)
8. M.E. Martínez-Klimov, P. Hernandez-Hipólito, T.E. Klimova, D.A. Solís-Casados, M. Martínez-García, J. Catal. **342**, 138 (2016)
9. K.R. More, R. Mali, Tetrahedron **72**, 7496 (2016)
10. J.L. Pratihar, P. Mandal, C.-H. Lin, C.-K. Lai, D. Mal, Polyhedron **135**, 224 (2017)
11. A.R. Hajipour, Z. Khorsandi, Catal. Commun. **77**, 1 (2016)
12. S.S. Shendage, A.S. Singh, J.M. Nagarkar, Tetrahedron Lett. **55**, 857 (2014)
13. D. Sahu, C. Sarmah, P. Das, Tetrahedron Lett. **55**, 3422 (2014)
14. A. Guarnizo, I. Angurell, G. Muller, J. Llorca, M. Seco, O. Rossell, M. Rossell, RSC Adv. **6**, 68675 (2016)
15. S. Verma, D. Verma, A.K. Sinha, S.L. Jain, Appl. Catal. A **489**, 17 (2015)
16. X.-D. Xiao, Y.-L. Bai, J.-Q. Liu, J.-W. Wang, Tetrahedron Lett. **57**, 3385 (2016)
17. T. Taira, T. Yanagimoto, K. Sakai, H. Sakai, A. Endo, T. Imura, Tetrahedron **7**(2), 4117 (2016)
18. C.J. Madadrang, H.Y. Kim, G. Gao, N. Wang, J. Zhu, H. Feng, M. Gorring, M.L. Kasner, S. Hou, ACS Appl Mater Interfaces **4**, 1186 (2012)
19. J. Gou, Q. Ma, X. Deng, Y. Cui, H. Zhang, X. Cheng, X. Li, M. Xie, Q. Cheng, Chem. Eng. J. **308**, 818 (2017)
20. Y. Zhao, C. Tao, G. Xiao, G. Wei, L. Li, C. Liu, H. Su, Nanoscale **8**, 5313 (2016)
21. W. Puthai, M. Kanezashi, H. Nagasawa, T. Tsuru, J. Membr. Sci. **524**, 700 (2017)
22. J.C. Pessoa, M.R. Maurya, Inorg. Chim. Acta **455**, 415 (2017)
23. D. Bonduel, S. Bredeau, M. Alexandre. F. Monteverde, P. Dubois, J. Mater. Chem. **17**, 2359 (2007)
24. C. Ruiz-García, J. Pérez-Carvajal, A. Berenguer-Murcia, M. Darder, P. Aranda, D. Cazorla-Amorós, E. Ruiz-Hitzky, Phys. Chem. Chem. Phys. **15**, 18635 (2013)
25. Z. Zhang, B. Liu, K. Lv, J. Sun, K. Deng, Green Chem. **16**, 2762 (2014)
26. N. Mansor, T.S. Miller, I. Dedigama, A.B. Jorge, J. Jia, V. Brázdová, C. Mattevi, C. Gibbs, D. Hodgson, P.R. Shearing, Electrochimica Acta **222**, 44 (2016)
27. S.M. Sarkar, M.L. Rahman, M.M. Yusoff, New J. Chem. **39**, 3564 (2015)
28. M. Amini, M. Bagherzadeh, Z. Moradi-Shoeili, D.M. Boghaei, RSC Adv. **2**, 12091 (2012)
29. M. Heidarizadeh, E. Doustkhah, S. Rostamnia, P.F. Rezaei, F.D. Harzevili, B. Zeynizadeh, Int. J. Biol. Macromol. **101**, 696 (2017)
30. H. Li, X. Zhu, H. Sitinamaluwa, K. Wasalathilake, L. Xu, S. Zhang, C. Yan, J. Alloy. Compd. **714**, 425 (2017)
31. R.H. Fath, S.J. Hoseini, H.G. Khozestan, J. Organomet. Chem. **842**, 1 (2017)
32. J. Safari, S. Gandomi-Ravandi, S. Ashiri, New J. Chem. **40**, 512 (2016)
33. G.C. Dickmu, L. Stahl, I.P. Smoliakova, J. Organomet. Chem. **756**, 27 (2014)
34. K.A. Kumar, L. Chandana, P. Ghosal, C. Subrahmanyam, Mol. Catal. **451**, 87 (2017)
35. S. Mahalingam, J. Ramasamy, Y.-H. Ahn, J. Taiwan Inst. Chem. Eng. **80**, 276 (2017)
36. G. Yang, L. Li, R.K. Rana, J.-J. Zhu, Carbon **61**, 357 (2013)
37. J.Y. Park, S. Kim, Int. J. Hydrog. Energy **38**, 6275 (2013)
38. G. Wu, X. Wang, N. Guan, L. Li, Appl. Catal. B **136**, 177 (2013)
39. A.R. Siamaki, S.K. Abd El Rahman, V. Abdelsayed, M.S. El-Shall, B.F. Gupton, J. Catal. **279**, 1 (2011)
40. F.R. Fortea-Pérez, M. Julve, E.V. Dikarev, A.S. Filatov, S.-E. Stiriba, Inorganica Chimica Acta (2017)
41. S.D. Dindulkar, D. Jeong, H. Kim, S. Jung, Carbohydr. Res. **430**, 85 (2016)
42. M. Amini, D.B. Heydarloo, M. Rahimi, M.G. Kim, S. Gautam, K.H. Chae, Mater. Res. Bull. **83**, 179 (2016)
43. E. Rafiee, M. Kahrizi, J. Mol. Liq. **218**, 625 (2016)
44. F. Ashouri, M. Zare, M. Bagherzadeh, C. R. Chim. **20**, 107 (2017)